Hyperfine Interact (2006) 170:131–143
DOI 10.1007/s10751-006-9463-6

Studying surfaces and thin films using Mössbauer spectroscopy

Laura K. Perry · D. H. Ryan · R. Gagnon

Abstract Using a series of bi-layer samples, we show how Conversion Electron Mössbauer Spectroscopy (CEMS) and X-ray Backscatter Mössbauer Spectroscopy (XBS) can be done with the same experimental set up. The penetration depths of the K and L conversion electrons are measured as 51(6) and 330(240) nm, respectively, with relative contributions of 88(9) and 12(9)%. The penetration depth of the Fe-K_α X-ray signal is determined to be 3.6(2) μm. As a demonstration we show data on surface damage effects in electropolished TRIP steels, and by comparing CEMS and XBS Mössbauer patterns we estimate the thickness of a damaged layer (created by sanding) to be 550(50) nm.

Key words Mössbauer spectroscopy · CEMS · XBS · Thin films · K conversion electrons · L conversion electrons · X-ray backscattering

1 Introduction

Conventional transmission Mössbauer spectroscopy is used to study bulk sample properties: magnetic, chemical and structural. Resonance is detected by the loss of transmitted intensity, giving an absorption spectrum. Each resonant absorption event creates a nucleus in an excited state, and this nucleus must return to the ground state by re-emitting radiation (γ-ray, X-ray, conversion electron and auger electron). These backscattered radiations are used in conversion electron Mössbauer spectroscopy (CEMS) and X-ray backscattering (XBS).

CEMS and XBS are backscattering methods in which the detected signal comes from the incident face of the sample. A backscattering approach is attractive if

L. K. Perry (✉) · D. H. Ryan · R. Gagnon
Center for the Physics of Materials, Department of Physics,
McGill University, Rutherford Building, 3600 University Street,
Montréal, Québec, Canada H3A 2T8
e-mail: perryl@physics.mcgill.ca

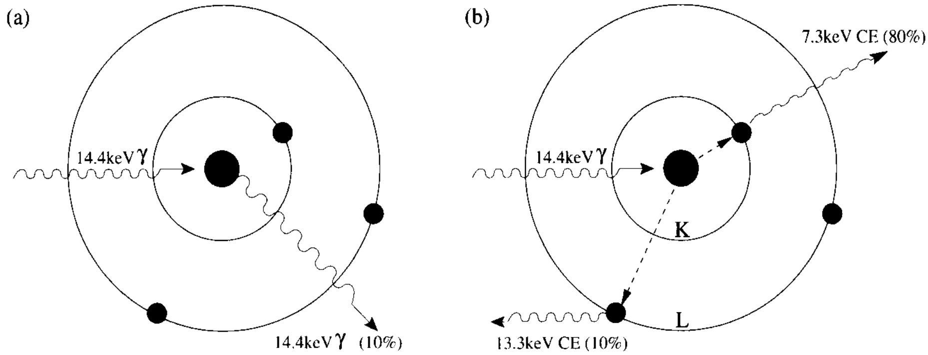

Figure 1 Internal processing of incident γ-radiation in ^{57}Fe. The nucleus may **a** re-emit a 14.4 keV γ-ray (10%) or **b** transfer the energy to shell electrons through virtual photons, emitting K-level (7.3 keV at 80%) and L-level (13.3 keV at 10%) conversion electrons [4].

the sample is either too thick (where the transmission signal would be completely absorbed), too thin (where absorption is negligible), or where the surface is the focus of the investigation. The penetration depths of conversion electrons and X-rays are much lower than γ-rays, and thus the backscattered signal must come from events close to the surface in order to be detected. This makes both CEMS and XBS surface-biased techniques, yielding Mössbauer spectra with all of the conventional magnetic, chemical and structural information, but derived from nuclei close to the sample surface. Because conversion electrons are less penetrating than X-rays, CEMS is more surface-biased than XBS and is the conventional method chosen to study surfaces and thin films. X-rays can escape from deeper within the sample and thus give more information on bulk sample properties.

Combining CEMS and XBS data on the same sample allows surface (~120 nm) and deeper (~8,100 nm) contributions to be distinguished. In this study, we examine bi-layered samples consisting of a thin iron overlayer (ranging between 17(1) nm and 6.1 μm) on a 304 stainless steel substrate, through CEMS and XBS. The difference between the Mössbauer patterns of non-magnetic stainless steel and magnetic iron motivates this choice of sample, because it allows the CEMS and XBS signals arising from each material to be distinguished. As an example of application, we show data on surface damage effects in electropolished TRIP steel, an alloy with magnetic and non-magnetic phases and thus whose Mössbauer pattern resembles that of the bi-layered samples. Through CEMS and XBS, the surface and bulk of TRIP steel can be studied, and since the surface is very sensitive to damage, comparing the two methods can provide insight into optimal surface preparation techniques. The penetration depths of conversion electrons and X-rays in iron are used to determine the thickness of a damaged layer created by sanding a TRIP steel surface.

2 Conversion electron Mössbauer spectroscopy

When incoming γ-radiation excites ^{57}Fe to its first excited state at 14.4 keV, the nucleus can shed the extra energy through several means. One of these processes, shown in Figure 1a, is the re-emission of a 14.4 keV γ-ray (10% probable). This

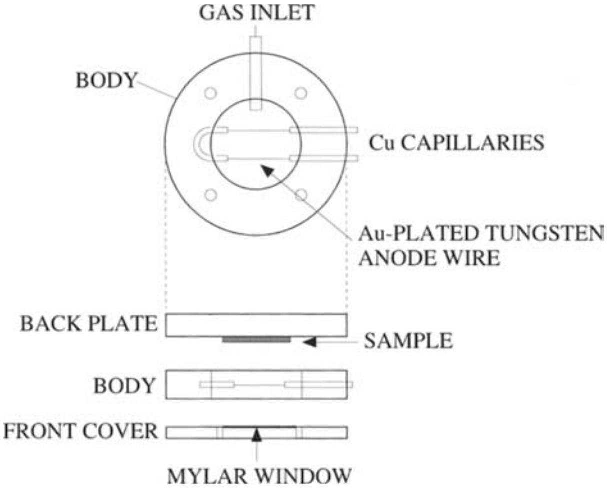

Figure 2 Sectional views of the CEMS detector. The *top diagram* illustrates a section through the anode plane, and the *bottom* shows a side view of the separate components.

backscattered γ-radiation is used in selective excitation double Mössbauer spectroscopy (SEDM) [1, 2], and can also be used as another means of backscattering Mössbauer spectroscopy (instead of CEMS and XBS) [3]. The more probable process is shown in Figure 1b, in which the nucleus transfers the energy to a 1*s* or *K* shell electron through a virtual photon, resulting in the emission of a 7.3 keV conversion electron (80% probable), or to a 2*s* or *L* shell electron, emitting a 13.3 keV conversion electron (10% probable). The energy of the outgoing radiation is given by $E_{CE} = E_\gamma - E_B$, where E_B is the binding energy of that shell. All probabilities are from [4].

Conversion electrons are detected through Conversion Electron Mössbauer Spectroscopy (CEMS [5]). A Mössbauer spectrum arises because the backscattered radiation is new radiation emitted at resonance. As the 7.3 keV electrons penetrate through very little matter, they are only detected when they are emitted near the surface of a sample. CEMS is most often chosen because of this bias to the sample surface, and is commonly used on thin films and treated surfaces [6, 7], as well as in corrosion studies. Since CEMS is a backscattering method, it is also a possible approach when a sample is too thick to be evaluated through transmission Mössbauer spectroscopy, where the beam is entirely absorbed in the thick material.

2.1 CEMS detector design

Since conversion electrons have shallow penetration depths (90% of the *K*-conversion electron signal comes from the first ~120 nm of the sample), there can be no window between the sample and detector, as any window material would stop the electrons before they could enter the detector. Most events occur too deep to be detected, so the count rate is low. In addition, those events occurring near the surface often are not detected because the electron emission is in the wrong direction. Detector efficiency is therefore key in the design of the CEMS detector.

The CEMS detector shown in Figure 2 is a continuous-flow gas-filled proportional counter, similar in design to the detector built by Liao et al. [8]. Alternate CEMS detector designs are given by [5, 9]. The detector has three main parts: a front

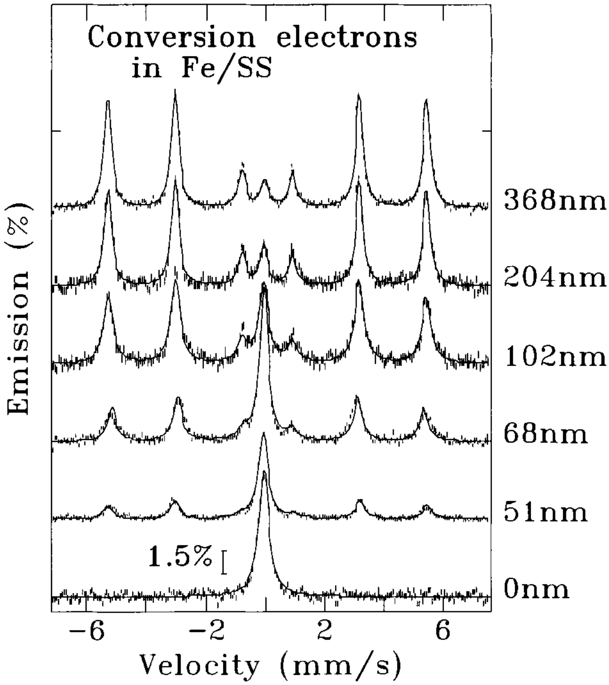

Figure 3 Conversion electron Mössbauer spectra of Fe/SS for a range of Fe overlayer thicknesses of 17(1) to 368(1) nm. At 368(1) nm, the magnetic peaks of Fe dominate the spectrum.

window (0.7 mm thick Plexiglass), a body and a backplate, and all of the inner surfaces are coated with aluminum and connected to ground. The ^{57}Co Mössbauer source emits not only 14.4 keV γ-rays, but also 6.4 keV Fe-K_α X-rays, which produce a background signal of photoelectrons. Photoelectrons are also produced when non-resonant 14.4 keV γ-rays and higher energy photons scatter from non-resonant materials [8]. The detector body is thus made of Plexiglass, because low Z materials help to reduce photoelectron production. The body carries the anode wire, the high voltage connection, and the fill gas line. The 25 μm anode wire is made of tungsten, for strength under tension, and plated with gold to avoid corrosion and contamination. A voltage of ~1000 V is applied to the anode. Lower voltages produce lower gain, while higher voltages cause breakdown. The sample is mounted on the backplate, with the sample surface directly exposed to the gas flow [5]. The fill gas used in the proportional counter is 4%CH_4/He. Helium is chosen as the primary gas because it is transparent to most radiation except conversion electrons. For instance, at atmospheric pressure, a 3.5 mm thick He gas layer has efficiencies of less than 0.02% for 6.4 keV X-rays and less than 0.002% for 14.4 keV γ-rays [10]. The fill gas is pre-mixed with CH_4, a quench gas that is present to absorb de-excitation photons emitted when collisions between electrons and neutral gas atoms excite the gas atoms. It thus stabilizes the proportional region of the detector. The flow rate was approximately 30 ml/min.

2.2 Conversion electron ranges in Fe

Mössbauer spectra were collected using a 3.7 GBq Rh ^{57}Co source mounted on a constant-acceleration spectrometer, calibrated using α-Fe foil at room temperature.

Figure 4 Natural logarithm of the stainless steel signal vs. Fe overlayer thickness for conversion electrons. The K-conversion electrons are attenuated by shallower overlayer thicknesses than L-conversion electron. This introduces a break in slope where the L-conversion electron signal starts to dominate over that of the K-conversion electrons.

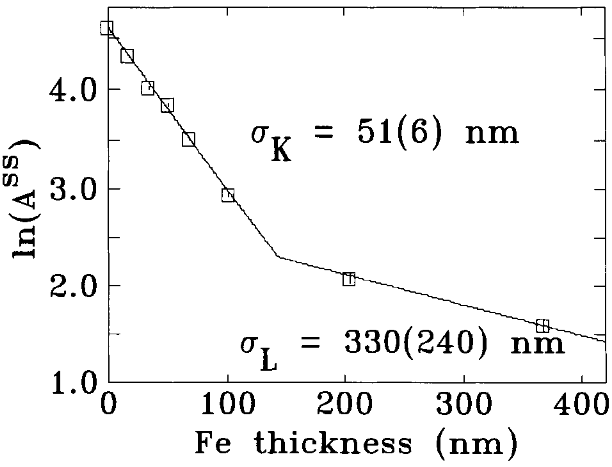

Table I Binding energies, conversion electron energies, penetration depths and emission probabilities of K- and L-conversion electrons in Fe/SS (from CEMS)

Shell	E_B (keV)	E_{CE} (keV)	σ (nm)	% Probability
K	7.1	7.3	51(6)	88(9)
L	0.7	13.3	330(240)	12(9)

Typical count rates were 300 counts per second. The iron films were deposited at room temperature by DC-magnetron sputtering onto non-magnetic 304 stainless steel substrates. We used an argon pressure of 1 x 10^{-2} torr and a power of 50 W, leading to a deposition rate of around 5 nm/min. The overlayer thicknesses were estimated using this deposition rate, then determined by X-ray reflectivity. The iron film thicknesses varied from 17(1) to 368(1) nm.

Figure 3 shows the conversion electron Mössbauer spectra of Fe/SS for overlayer thicknesses ranging between 17(1) and 368(1) nm. The central stainless steel peak rapidly decreases in intensity as the overlayer thickness increases. This is due to a shift in balance between the substrate and overlayer signals, where at thick overlayers, the iron signal dominates. The stainless steel conversion electron signal decreases as $A^{ss} = A_o^{ss} e^{-d/\sigma}$, where A_o^{ss} is the initial stainless steel area for zero overlayer thickness, A^{ss} the measured stainless steel area, d the overlayer thickness, and σ the penetration depth of conversion electrons in iron. Figure 4 shows the natural log of A^{ss} as a function of overlayer thickness, and the inverse of the slope gives the penetration depth. The rapidly attenuated part is due to the K-conversion electrons (7.3 keV), which have a lower penetration depth than L-conversion electrons (13.3 keV) but a higher emission probability. The slowly attenuated part, due to the L-conversion electrons, dominates at thicknesses greater than 200 nm because the K-conversion electrons are greatly attenuated by the thicker overlayers. The measured penetration depths are 51(6) nm for K-conversion electrons and 330(240) nm for L-conversion electrons (Table I).

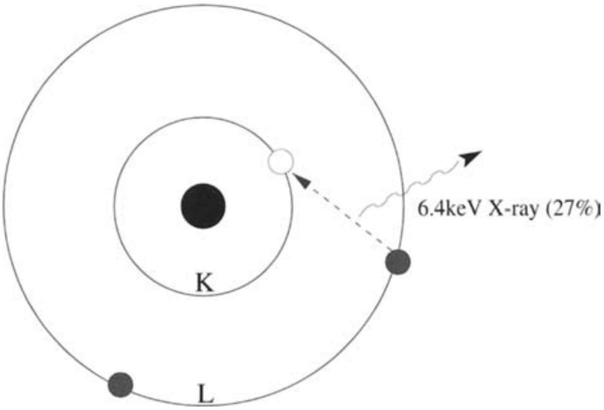

Figure 5 An L shell electron falls to fill the hole on the K shell introduced by the K-conversion electron emission. This creates a 6.4 keV X-ray (27%), or a 5.6 keV Auger electron (63%) [4].

3 X-ray backscattering

When the nucleus is excited by incident 14.4 keV γ-radiation, the energy can be transferred to a K shell electron by means of a virtual photon, emitting a K-conversion electron (Section 2). The void created by the loss of the K shell electron is filled by an L shell electron, and the decay from higher to lower shell causes the emission of an X-ray with an energy corresponding to the difference in binding energy of the electronic shells (Figure 5). In the case of ^{57}Fe, the difference in binding energies of the K and L shells is 6.4 keV, which is the Fe-K_α that is used in X-ray backscattering (XBS).

The main difference between CEMS and XBS is that X-rays are far more penetrating than conversion electrons, so that XBS is not as much a surface-sensitive technique. Due to the greater range of X-rays, the space between sample and detector is not as much a concern as in the case of CEMS. This allows for more liberty in sample location, because although the sample can be mounted in the detector chamber, it can also be located outside the detector chamber without losing the X-ray signal. Overall, XBS yields all the same information about a sample as would CEMS, but with lesser surface bias (90% of the XBS signal comes from the first ~8,100 nm of the sample, instead of ~120 nm for conversion electrons).

3.1 XBS detector design

The initial design of an Fe-K_α X-ray detector used a forward-scattering geometry which allowed the scattered X-rays to be detected in a solid angle of up to 2π [11]. The first appearance of an XBS detector was given by Swanson et al. [5] 3 years later in 1970. The XBS detector was then later designed to also count both X-rays and conversion electrons simultaneously [12], and eventually transmission γ-rays are also included [10, 13]. The detector used for XBS in this study is the same continuous-flow gas-filled proportional counter as that described in Section 2.1, save for a few details. The biggest concern are the Fe-K_α X-rays incident from the source. The source emits even more X-rays than γ-rays (Figure 6a), and being that the detector is now sensitive to X-rays, a proper filter must be chosen. A Plexiglass filter 3–4 mm thick nearly eliminates the incident X-ray intensity while only slightly reducing the

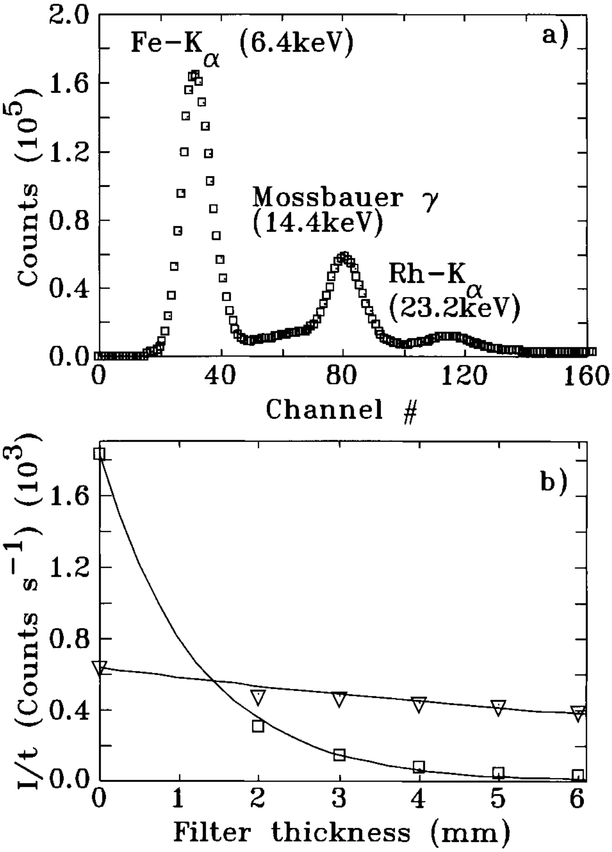

Figure 6 **a** Pulse height pattern of radiations emitted from the ^{57}Co source. There are 6.4 keV Fe-K_α X-rays, 14.4 keV γ-rays, and 23.2 keV Rh-K_α X-rays. **b** X-ray and γ-ray intensity (divided by time) for varying Plexiglass filter thicknesses.

γ-ray intensity (Figure 6b). The fill gas used is 10%CH_4/Ar. The absorption depth of 6.4 keV X-rays in Ar is on the order of 3 cm, and that of 14.4 keV γ-rays is 25 cm [14]. The primary component of the fill gas is therefore chosen to be Ar because it has a higher X-ray stopping power than He, while being transparent to the 14.4 keV γ-rays. The flow rate was approximately 30 ml/min.

A side view of the CEMS/XBS detector is shown in part (a) of Figure 7, with the sample mounted inside the detector chamber. Since Ar has a higher stopping power than He, both X-rays *and* conversion electrons are detected in the detector chamber. The detector energy window set by the signal channel analyzer (SCA) is narrowed around the 6.4 keV X-ray. The K-conversion electrons (7.3 keV) emitted by the sample are similar in energy to X-rays, and they too are detected in this energy range and contribute approximately 20% to the overall signal. In part (b) of Figure 7, the detector's backplate was replaced by an aluminized Mylar window. The sample was mounted behind the Mylar window, outside of the detector chamber. This eliminated the conversion electron signal that appeared in the former setup.

3.2 X-ray range in iron

In addition to the sputtered samples described in Section 2.2, iron foil was used as an added overlayer. The iron foil was made by Goodfellow and is 99.85% pure, with

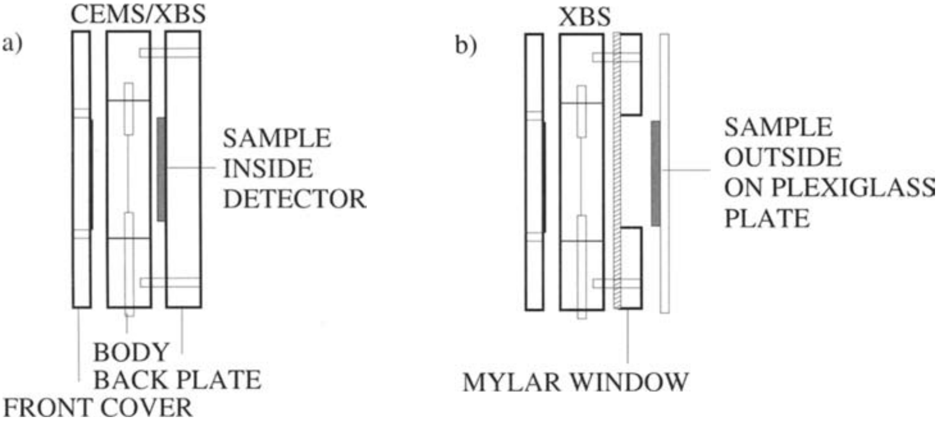

Figure 7 **a** Side view of the CEMS/XBS detector, with the sample mounted inside the detector chamber. **b** Side view of the XBS detector with the sample mounted outside to eliminate contaminant conversion electrons.

Figure 8 X-ray backscattering Mössbauer spectra of Fe/SS for a range of Fe overlayer thicknesses of 368(1) to 6083 nm. To reduce the stainless steel spectral area, the overlayer thickness must be larger than that required to attenuate the less penetrating conversion electrons.

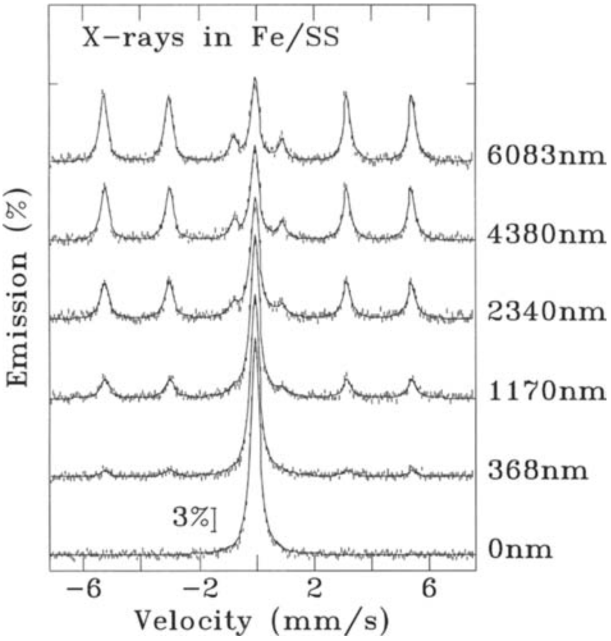

dimensions 50 × 50 × 0.001 mm. The overlayer thicknesses varied from 17(1) nm to 6.1 μm. Thicker overlayers are needed due to the greater range of Fe-K_α X-rays. Typical count rates were 100 counts per second.

Figure 8 shows XBS Mössbauer spectra, with Fe overlayer thicknesses ranging between 368(1) nm and 6.1 μm. On comparison with Figure 3, we immediately see that a greater overlayer thickness is required to attenuate the XBS signal from stainless steel. Even at 368 nm, the magnetic Fe peaks are only just beginning to

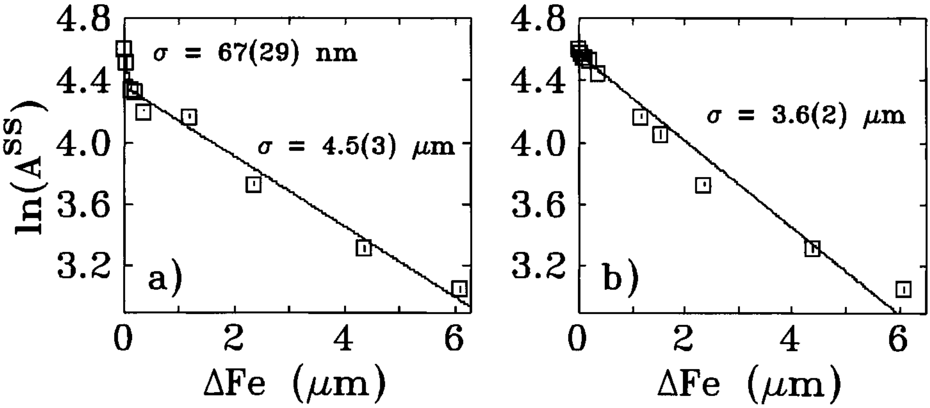

Figure 9 Natural logarithm of the percent stainless steel signal vs. Fe overlayer thickness (ΔFe) for X-rays, with overlayer thicknesses ranging between 17(1) nm and 6.1 μm. **a** The sample is mounted inside the detector chamber, and the signal receives contributions from 6.4 keV X-rays (76(3)%) as well as surface conversion electrons (24(3)%). **b** The sample is mounted outside of the detector chamber, and the aluminized Mylar window between the sample and detector eliminates the conversion electron signal.

Table II Penetration depths and relative signal contributions of *K*-conversion electrons and X-rays in Fe/SS, as obtained through XBS and with the sample mounted inside and outside of the detector chamber. The % column shows the relative distribution of the different signals

RADIATION	Inside σ	%	Outside σ
K-level conversion e^-	67(29) nm	24(3)	-
X-ray	4.5(3) μm	76(3)	3.6(2) μm

appear. This illustrates the greater penetrating power of X-rays as compared to conversion electrons.

Figure 9 shows the natural log of the stainless steel signal area (A^{ss}) for overlayer thicknesses ranging between 17(1) nm and 6.1 μm. In part (a) of Figure 9, the sample was mounted inside the detector (Figure 7a), and a break in slope appears at ~90 nm. The penetration depth obtained from the most rapidly attenuated contribution is 67(29) nm, which is within error of the *K*-conversion electron range of 51(6) nm determined in Section 2.2. For part (b) of Figure 9, the sample was mounted outside the detector, and an aluminized Mylar window stops the *K*-conversion electrons from entering the detector (Figure 7b) so that only the X-rays contribute. The penetration depth of X-rays in iron was determined to be 3.6(2) μm. Table II summarizes the results for XBS.

4 Application to TRIP steel

When an austenitic steel is plastically deformed at room temperature, some of the austenitic phase (solid solution of carbon in FCC or γ-Fe) in the most severely strained portions of the steel will transform to martensite (BCC form of iron in which some carbon is dissolved). TRIP is an acronym for the **TR**ansformation **I**nduced

Plasticity of a metal alloy, and the strain-induced decomposition of the austenitic phase is an important contributor to the observed properties of the alloy [15]. The term *retained austenite* refers to the stabilization of residual austenite by the carbon that is partitioned from bainitic ferrite [15]. A typical phase composition consists of 10% retained austenite (face-centered cubic), 20% bainitic ferrite (body-centered cubic) and balance allotriomorphic ferrite [16]. In short, TRIP steel consists of small austenitic inclusions in a ferrite matrix.

The distinguishing characteristic of the FCC austenitic phases is that they are non-magnetic. The Mössbauer pattern of austenite is thus a single peak, whereas that from the ferritic phases consists of six peaks, typical of magnetic iron-bearing alloys. This closely resembles the bi-layered samples examined by CEMS and XBS in Sections 2 and 3, where the Mössbauer patterns consisted of a single peak for stainless steel and six peaks for magnetic iron.

A common approach to determining the amount of retained austenite in a TRIP steel is Cu-K_α X-ray diffraction (XRD). When a sample is evaluated through XRD, even at normal incidence the X-ray signal from a depth d in the sample must make two passes through that thickness prior to detection (one upon incidence and another upon escape), so that the overall travel path length is $2d$. In contrast, the XBS X-ray originates from within the sample itself, and makes only a single pass through d before escaping. Furthermore, the 6.4 keV Fe-K_α and the 8.05 keV Cu-K_α X-rays lie on either side of the iron K edge at 7.11 keV. Considering the total attenuation of the Cu-K_α X-ray (297.80 cm^2/g compared to 70.34 cm^2/g for Fe-K_α X-rays) and the amount of material through which it must pass for detection, Cu-K_α X-rays are least eight times more attenuated by iron than Fe-K_α X-rays. Consequently, the majority of Cu-K_α XRD signals come from the surface of the sample, and as the TRIP steel surface is highly sensitive to damage, XRD may not be as reliable a technique for determining the bulk retained austenite fraction as Fe-K_α XBS.

TRIP steels are prone to surface damage because the austenitic phases readily transform to martensite under stress. Samples for phase analysis are often cut from larger billets, therefore any method which probes only surface properties, such as Cu-K_α X-ray diffraction and CEMS, will underestimate the retained austenite fraction because the surface phases are destroyed. To a certain extent, the damaged surface can be removed through electropolishing, a chemical etch intended to remove the damaged surface. However, bulk methods such as neutron diffraction and XBS are preferred because they depend less on the efficiency of surface preparation techniques. By comparing CEMS and XBS on the same TRIP steel sample, we explore surface damage effects and demonstrate that even simple mechanical working suffices to destroy the surface austenitic phases. Through XBS and CEMS measurements we obtain an estimate for the thickness of the damaged layer created through sanding.

4.1 Results

The CEMS and XBS Mössbauer spectra of an electropolished TRIP steel (with a ~7% retained austenite content) are shown in Figure 10 (left). They were fitted with three components: two magnetic (ferrite and martensite) and one non-magnetic (austenite). The difference in retained austenite fraction measured by CEMS and XBS (3.4(6) and 6.4(6)%, respectively, Table III) suggests that the damaged surface

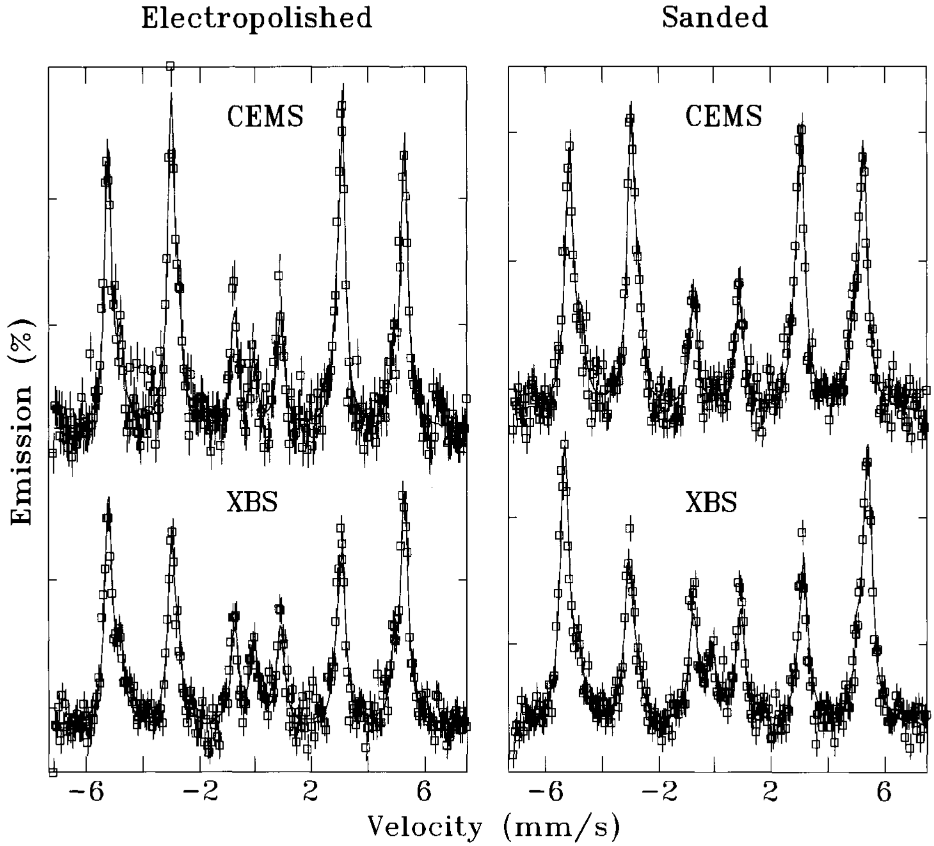

Figure 10 Conversion electron and X-ray backscattering Mössbauer spectra for TRIP steel, with electropolished and sanded surface.

has not been completely removed through electropolishing. Cu-K_α X-ray diffraction would give an even lower estimate of austenite content than CEMS, emphasizing the importance of the efficiency of surface preparation if surface-biased probes are used.

When the electropolished surface is sanded (600 grit sanding paper), a new damaged layer is created. The stress of sanding transforms the surface austenitic phases to martensite. Figure 10 (right) shows the CEMS and XBS Mössbauer spectra of the TRIP steel with the damaged surface. While the central austenitic component is present in the electropolished CEMS and XBS patterns (left), it survives only in the XBS pattern of the sanded TRIP steel (right). The central peak disappears completely in the right CEMS pattern, indicating that the surface is completely destroyed and that the damaged layer is at least 100 nm thick. The XBS patterns show only a 14% loss of austenite signal in going from electropolished to sanded surfaces, reinforcing this choice of method for the measurement of retained austenite fraction.

Table III lists the retained austenite content of the TRIP steel, from CEMS and XBS. In order to estimate the thickness of the damaged layer, we model the sanded TRIP steel as a bi-layered sample, with a damaged austenite-free surface layer overlaying bulk TRIP steel. The retained austenite fraction of the underlayer is estimated from XBS measurements on the electropolished surface. There are

Table III Conversion electrons and X-rays emitted from austenitic phases in TRIP steel, with electropolished and sanded surface. A^{aus} is the measured area of the austenitic phase (identical to A^{ss} from Sections 2.2 and 3.2). The conversion electron austenite signal is completely eliminated by the damaged layer created through sanding, and the X-ray signal is only slightly reduced

RADIATION	Setup	A^{aus} (%)	
		Electropolish	Sanded
X-rays	Inside	6.4(6)	5.1(9)
	Outside	-	5.5(5)
Conversion e$^-$'s	Inside	3.4(6)	0.9(5)

therefore two contributions to the overall signal: one from the bulk (6.4(6)% retained austenite), and another from the damaged surface (0% retained austenite). The overall XBS retained austenite fraction from both contributions is 5.5(5)% (Table III). The measured austenite area A^{aus} is given by $A^{aus} = A_o^{aus}e^{-d/\sigma}$, where A_o^{aus} is the initial austenite area in the absence of the damaged layer. The damaged layer thickness d can be obtained by integrating over the two contributions to A^{aus}:

$$x_o = x_d \int_0^d A_o^{aus}e^{-x/\sigma} + x_b \int_d^\infty A_o^{aus}e^{-x/\sigma} \tag{1}$$

where x_o is the overall retained austenite fraction (5.5(5)%), x_d is zero (the damaged layer contains no austenite), x_b is the retained austenite fraction of the bulk (6.4(6)%), and σ the penetration depth of X-rays in iron (3.6(2) μm). From this we obtain the damaged layer thickness d = 550(50) nm.

5 Conclusions

Through conversion electron Mössbauer spectroscopy and X-ray backscattering, we have determined penetration depths for conversion electrons and X-rays in iron. Both methods are easy and can be performed using the same detector, with only minor changes. For CEMS, the detector can distinguish between conversion electron contributions from different electronic shells, and for XBS, the detector can be tuned to detect only X-ray emissions. CEMS and XBS are both useful in determining the retained austenite content of a TRIP steel, and the comparison between the measured retained austenite fraction obtained by the two methods demonstrates the extreme surface sensitivity of the alloy. Simple mechanical working such as sanding is sufficient to create a damaged layer that is half a micron thick. Electropolishing does remove some of the surface damage, but it is preferable to use bulk methods such as Neutron scattering and XBS if the purpose of the study is to determine the retained austenite fraction.

References

1. Van Lierop, J., Ryan, D.H.: Rev. Sci. Instrum. **72**, 3349 (2001)
2. Van Lierop, J., Ryan, D.H.: Hyperfine Interact. **141/142**, 141 (2002)
3. Keisch, B.: Nucl. Instrum. Methods **104**, 237 (1972)

4. Liljequist, D.: Mössbauer spectroscopy with electrons. Scanning Electron Microsc. **3**, 997–1017 (1983)
5. Swanson, K.R., Spikerman, J.J.: J. App. Phys. **41**, 3155 (1970)
6. Schaaf, P., Bauer, P., Gonser, U.: Z. Metallkunde **80**, 77 (1989)
7. Bibicu, I., Rogalski, M.S., Nicolescu, G.: Phys. Status Solidi, B. **178**, 459 (1993)
8. Liao, L.X., Ryan, D.H., Altounian, Z.: Rev. Sci. Instrum. **64**, 679 (1993)
9. Bonchev, Z.W., Jordanov, A., Minkova, A.: Nucl. Instrum. Methods **70**, 36 (1969)
10. Bibicu, I., Rogalski, M.S., Nicolescu, G.: Meas. Sci. Technol. **7**, 113 (1996)
11. Hershkowitz, N., Walker, J.C.: Nucl. Instrum. Methods **53**, 273 (1967)
12. Isozumi, Y., Lee, D.-I., Kádár, I.: Nucl. Instrum. Methods **120**, 23 (1974)
13. Bibicu, I., Rogalski, M.S., Nicolescu, G.: Nucl. Instrum. Methods, B. **94**, 330 (1994)
14. McMaster, W.H., Del Grande, N.K., Mallett, J.H., Hubbell, J.H.: Compilation of X-ray cross sections, Sec. 2, Rev. 1. U.S. Atomic Energy Commission Report UCRL-50174, pp. 350. University of California, Livermore, USA (1969)
15. Sheriff, M.Y., Garcia Mateo, C., Sourmail, T., Bhadeshia, H.K.D.H.: Mater. Sci. Technol. **20**, 319 (2004)
16. Bhadeshia, H.K.D.H.: ISIJ Int. **42**, 1059 (2002)